Composites Part B 176 (2019) 107197

Contents lists available at ScienceDirect

Composites Part B

journal homepage: www.elsevier.com/locate/composites

Shredding and sieving thermoplastic composite scrap: Method development and analyses of the fibre length distributions

Guillaume A. Vincent [a,b], Thomas A. de Bruijn [c], Sebastiaan Wijskamp [b], Mohammed Iqbal Abdul Rasheed [a], Martin van Drongelen [a,*], Remko Akkerman [a]

[a] Group of Production Technology, University of Twente, 7522 NB Enschede, the Netherlands
[b] ThermoPlastic composites Research Center, Palatijn 15, 7521 PN Enschede, the Netherlands
[c] ThermoPlastic composites Application Center, Saxion University of Applied Sciences, M.H. Tromplaan 28, 7513 AB Enschede, the Netherlands

ARTICLE INFO

Keywords:
A. Discontinuous reinforcement
C. Statistical properties/methods
E. Recycling
Fibre length distribution

ABSTRACT

Recycling of thermoplastic composites has attracted considerable attention in the recent years. Several recycling solutions include shredding scrap to centimetre-sized flakes to retain long fibres, followed by a remanufacturing step that prevents fibre breakage. Determining the exact fibre length distribution (FLD) for these routes is crucial, as it is of importance for the processibility of the material as well as the mechanical performance of the recycled parts. In this paper, novel analysis methods are introduced to calculate FLDs based on photographs of flakes. The reliability of the method and of the sampling was found to be high. The relation between flake size and FLD was studied, showing that offcut layup barely influences the FLD in comparison to flake size. The effects of shredding settings and sieving were studied, showing a strong correlation between machine parameters and FLD, whereas the offcut size was found to have no effect on FLD.

1. Introduction

With the demand and production of continuous fibre thermoplastic composites (TPCs) rising in the aerospace industry, the volume of production scrap has also grown and is expected to continue to grow in the future [1]. This scrap material is generated over the course of several processing steps of, for instance, three of the main manufacturing routes of TPCs, as shown in Fig. 1. There, the top flow chart represents a route where unidirectional tape prepregs, are placed into a mould, in which they are subsequently post-consolidated and/or formed. The middle process route represents autoclave consolidation and forming of prepregs. In the bottom flow chart, the prepregs are press-consolidated and then formed, e.g. by stamping. The dark-grey arrows represent the steps that produce scrap in these three manufacturing processes. Although many operations generate scrap, the bulk of the scrap is composed of nested offcuts and trims in a consolidated form, which are therefore multi-layered and may have various layups, such as in Fig. 2a. In addition to the production scrap, end-of-life (EoL) TPC waste will later join the recyclable waste feed and become a critical issue. Recycling these streams is economically attractive because of the high value of composite waste and will probably become mandatory from an environmental perspective in the future. Several European directives have already put restrictions on disposal and require that specific waste streams be recycled [2,3].

Several recycling solutions specific to TPCs have been implemented in recent years to convert this production scrap [4–14]. They all follow the same scheme: size reduction, separation of impurities if necessary, and manufacturing a new part. In all cases, the recycled part is manufactured with a process that resembles compression moulding of discontinuous-fibre composites. In these various approaches, the desired fibre length ranges from sub-millimetre and centimetre scale. Besides, some of these recycling solutions require the addition of pristine polymer to the recyclate to reduce its fibre fraction [5,6,8,10], while other solutions enable processing at the input fibre fraction [4,7–9,11,12,14]. Cradle-to-cradle approaches have also been proposed by some authors [7]. These recycling approaches, except the one reported by Roux et al. [7], contain a mechanical size reduction step using shredders, cutting mills or hammer mills. These types of comminution processes offer a large range of possibilities in term of output size, from powder to centimetre-sized flakes [15], depending on the requirements of the recycling route. Recently, De Bruijn [5,6] has proposed a solution that aims to retain most of the value and mechanical performance of TPC production scrap, consisting of shredding scrap to centimetre-long flakes, melting and mixing those flakes into a dough using a low-shear mixer, and transferring the dough to a press for compression moulding. Long fibres, and therefore large flakes, are required to achieve high

* Correspondence to: University of Twente, Faculty of Engineering Technology, Horst Complex N212, P.O. Box 217, 7500 AE Enschede, The Netherlands.
E-mail address: m.vandrongelen@utwente.nl (M. van Drongelen).

https://doi.org/10.1016/j.compositesb.2019.107197
Received 25 February 2019; Received in revised form 6 June 2019; Accepted 12 July 2019
Available online 15 July 2019

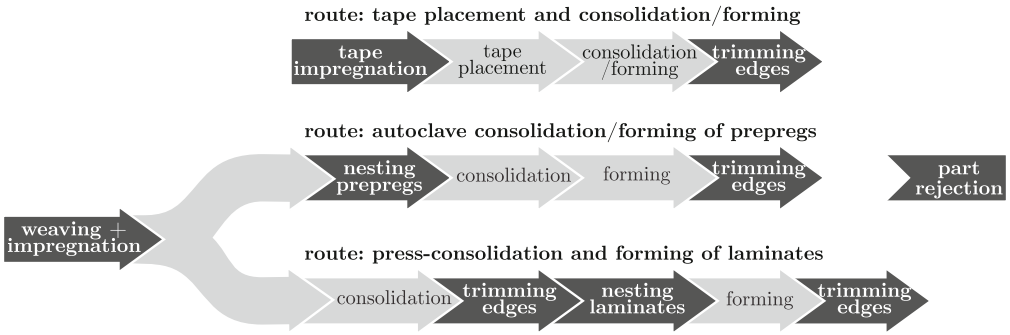

Fig. 1. Overview of the various main streams of production scrap during the manufacturing of TPCs. The light-grey boxes represent the various processing steps, whereas the dark-grey boxes highlight the operations where scrap is generated.

mechanical performance [16]. In addition, this solution is capable of processing consolidated scrap, which represents the bulk of production scrap, discarded components and EoL TPC waste.

In this recycling route, the micro-structure of recycled composite parts consists of entangled bundles instead of overlapping flakes such as in [4]. Both the flow behaviour of the dough during compression moulding and the mechanical properties of the recycled part will depend, among other parameters, on the fibre length distribution (FLD) [17]. As this recycling solution was developed in order to avoid breaking fibres during processing, it is important to determine the FLD of the shredded flakes rather than just the flake sizes, or particle size distribution (PSD).

Additionally, industrial applications of this recycling route may require tailored materials with specific flow behaviour or a certain part performance, in order to manufacture of certify a particular part. The production of various FLDs, with short or long fibres, with narrow or wide distributions, is an important criterion here. It is therefore essential to understand which factors influence the FLD and how to tailor these to specific requirements.

The literature already presents several methods to characterise the FLD, which can be categorised as direct and indirect. Methods are considered direct when all fibres in a sample are measured, whereas indirect methods only produce an estimated FLD. Direct measurements have been extensively used for short-fibre composites [18]. A typical example is injection moulding, where many fibre-length characterisations are carried out to determine fibre length reduction. In a significant share of these direct measurement methods, fibres are reclaimed by burning off the matrix, for instance, after which they are spread out on a piece of paper or scanner to be captured in a photograph. Image analysis is performed to determine the exact FLD [18,19]. This methodology works well for fibres of moderate length (length/diameter (L/D) < 1000). Longer fibres may bend considerably or overlap, which makes characterisation difficult. The latter method has been widely used for thermoset-composite recycling processes, particularly because the fibres are separated from the matrix during the process anyway [20–22]. However, many studies stopped characterising reclaimed long fibres ($L/D > 1000$) and started investigating flakes obtained from the size reduction process instead. This is primarily due to the image analysis methods used, as their technical limits are stretched at these lengths. For such long fibres, indirect measurements methods are used instead. In the case of recycling fibre-reinforced plastics, shredded scrap is sorted using sieves or air classifiers [23,24] and the PSD is obtained based on the sorted output. The FLD is estimated indirectly by being considered equal to the PSD. This may be true [24–29] for flakes in slender cured bundles form, as particle length is equal to fibre length in this case. However, when the output flakes have an aspect ratio close to unity, such as in [6] and as shown in Fig. 2b, the FLD can be far apart from the PSD [30]. This is mostly the case when fibre orientations differ from the principal directions of the flakes, in which case the FLD may not be approximated to the flake length. Therefore, in addition to the PSD, an alternative method is required to determine the FLD of large, possibly multi-layered, flakes. To the knowledge of the authors, this problem has, thus far, not been tackled.

Table 1
List of the offcut types used in this study. The widths and lengths are averages.

Category	Average weight [g]	Width [mm]	Length [mm]	Smallest dimension [mm]
C/PPS offcuts — small	8	60	150	20
C/PPS offcuts — medium	164	160	420	50
C/PPS offcuts — large	328	260	760	70
C/PPS offcuts — 2nd type	n/a	50	700	80

The objectives of this article are: 1. to develop and implement a reliable method that calculates the FLD based on a batch of multi-layered flakes; 2. to understand the relations between flakes and FLD to determine whether flake shape, size and layup affect the resulting FLDs; and 3. to understand whether and how offcut size, shredding settings and sieving can influence the FLD of the resulting flakes.

The current paper will elaborate on these three issues. Firstly, details on the materials, shredding/sieving processes, and the implemented method will be presented, followed by a results and discussion section, which will answer the objectives of this article.

2. Materials

The offcuts used in this article were collected at various manufacturing plants. For the purpose of this study, offcuts are defined as the remainders from the nesting or trimming stage of from prepregs or laminates (see Fig. 1). However, the offcuts collected in this study only consist of trims from the stamp-forming stage (shown in Fig. 2a), and trims from the press-consolidation stage (later referred as *offcut 2nd type*). Both types of offcuts consist of TenCate Cetex® TC1100 carbon/PPS (C/PPS) 5-harness satin consolidated in a quasi-isotropic layup, as shown in Fig. 2a. The trims from the stamp-forming stage were arbitrarily classified into three categories based on their offcut weight and are listed in Table 1. The second type of offcuts was not categorised because the offcuts in question were very similar in terms of size and is named: *C/PPS offcuts - 2nd type*. The trims collected in this study are composed of quasi-isotropic laminates as stated above. However, this will not always be the case, as the industry can use various layups to manufacture components.

Multiple shaft shredding was the size reduction method of choice for this study for its ability to produce large and uniform flakes unlike other technologies, such as hammer mills or cutting mills [31]. Two- and four-shaft shredders manufactured by UNTHA shredding technology Gmbh (hereinafter UNTHA) were used for this purpose. This type of machine was designed to shear the input material rather than impact it, as in hammer mills, which is achieved by having the shafts rotate at low speeds [31–33]. Practical experience of UNTHA and a project partner,

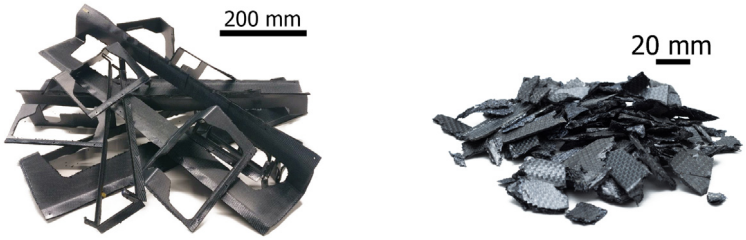

(a) C/PPS offcuts prior to shredding (b) C/PPS flakes obtained after shredding

Fig. 2. Pictures of scrap material before and after shredding.

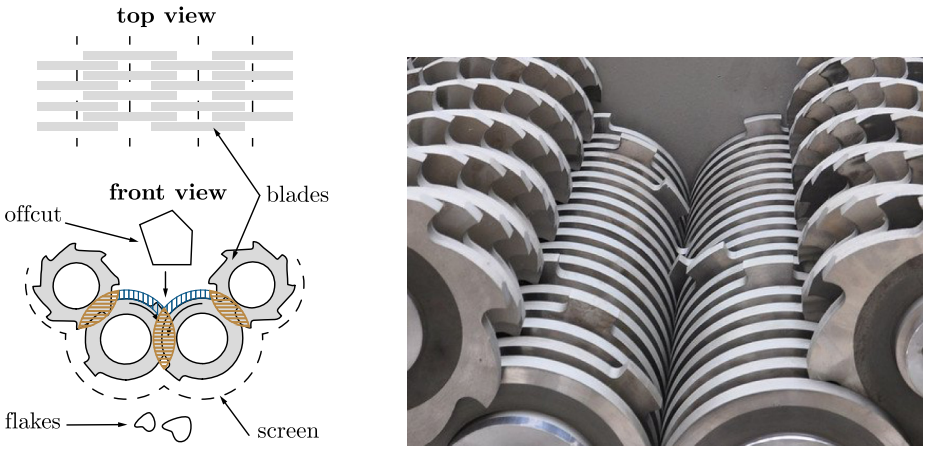

Fig. 3. Schematics of a shredder, top and front views in 3a, and inside view of a four-shaft shredder (image courtesy of UNTHA) in 3b.

Nido RecyclingTechniek, had shown that these machines produce a small fraction of fine particles compared to single-shaft shredders or hammer mills. Here, fine particles are defined as being five to ten times smaller than the intended main output of a machine. Most flakes are therefore in the desired size range, as one can see in Fig. 2b. The comminution mechanism of these shredders can be summarised as follows. The incoming material falls into the shredder, where teeth located on rotating blades force it to move downwards (see the blue vertically hatched areas in Fig. 3a). The rotating blades overlap and therefore shear the material in the orange horizontally hatched area in Fig. 3a. When a screen is placed directly beneath the blades, the flakes will either, fall through the screen, if they are small enough, or be caught by the teeth on the outer shafts, after which they are moved upwards to be shredded again. Obviously, blade width and screen size will influence the PSD. Apart from these two parameters, previous work on size reduction showed that the clearance between blades, small variations in rotational speed or sharpness of the blades/teeth have a major influence on the fracture mechanism but seem to have very little influence on the PSD [31]. Consequently, only the influence of blade width and screen size will be studied here. Various UNTHA shredders were used, depending on desired machine setting and availability, namely S20, RS30, RS40 and RS50. A summary of the shredding tests and the settings used is listed in Table 2. Apart from the blade width and screen size, shaft diameter, maximum torque, maximum throughput and number of shafts varied [32,33]. The first three are known to affect the input volume and size, but not the PSD *a priori*. Similarly, four-shaft shredders allow the machine to be auto-cleaned, whereas the two-shaft shredder (S20) does not, but no variation in PSD is expected.

Shredding experiments performed in collaboration with Nido RecyclingTechniek and UNTHA were found to produce very limited amounts of dust. The amount of dust in a workplace, especially when it comes to fibre-reinforced composites, must comply with the guidelines of the European Scientific Committee of Occupational Exposure Limits, which recommends that workers are not exposed to more than 1 fibre/cm^3 per 8-h time-weighted average (8-h TWA) [34]. RPS B.V. (Delft, the Netherlands), an external company certified to measure particles in workplaces, was commissioned to carry out a study on our S20 shredder to measure its small carbon fibre emissions when shredding the same C/PPS offcuts used in this study. The objective was to confirm or disprove the limited dust production with this comminution method and TPC material. Workers were given personal air sampling pumps and several stationary air pumps were installed in the lab during the

Fig. 4. Photograph of the multi-stage vibrating sieves used in this study.

Table 2
List of the various performed shredding tests. Section 4 will refer to the tests numbers listed here.

Test number	Scrap type	Blade width [mm]	Aperture of the screen [mm]	Shredder	Remarks
#1	C/PPS small	19	n/a	S20 (2-shaft)	No screen, 5 cuts
#2	C/PPS medium	19	n/a	S20 (2-shaft)	No screen, 5 cuts
#3	C/PPS large	19	n/a	S20 (2-shaft)	No screen, 5 cuts
#4	C/PPS large	29	25	RS50 (4-shaft)	1 cut
#5	C/PPS large	19	40	RS40 (4-shaft)	1 cut
#6	C/PPS large	29	40	RS50 (4-shaft)	1 cut
#7	C/PPS large	29	n/a	RS50 (4-shaft)	No screen, one cut
#8	C/PPS 2nd type	19	40	RS30 (4-shaft)	5+2 batches
#9	C/PPS large	19	n/a	S20 (2-shaft)	No screen, 5 cuts, used for sieving

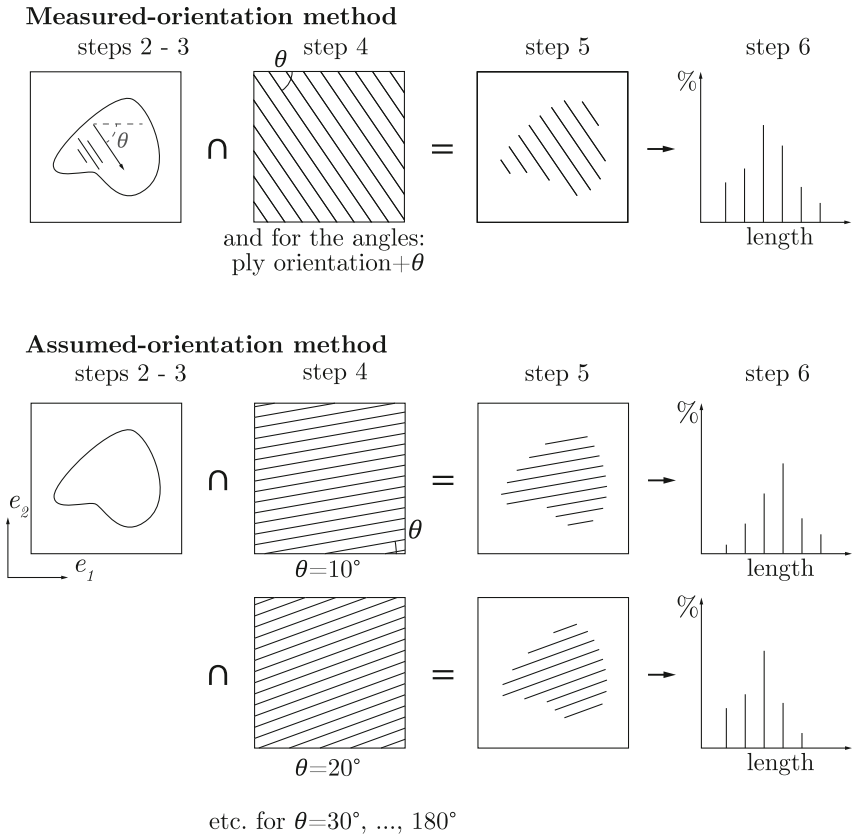

Fig. 5. Sketch of the process steps for the measured-orientation (top) and assumed-orientation (bottom) analysing methods. Step numbering refers to the process description in Section 3.

measurements to record dust exposure. All fibre exposure measurements were found to be below 1% of the 8-h TWA limit, which is a considerable safety advantage, showing the benefits of shredding thermoplastic composites. In comparison, Nido RecyclingTechniek and UNTHA had previously experienced that shredding and grinding thermoset composites produced large amounts of dust. The volume of dust generated during the thermoset composite shredding process was not measured.

After shredding, a 6 kg batch of shredded flakes was sieved using multi-stage vibrating sieves (see Fig. 4). A set of perforated-plate sieves and woven wire sieves, specified by ASTM E323 and ASTM E11 respectively, were used with the following sizes: 2, 2.8, 4, 5.6, 8, 11.2, 16, 22.4 and 31.5 mm. The PSD of sieved flakes is evidently correlated to the aperture of the sieve [23] but the exact relation is unknown, and the same goes for FLD and sieves. This study aimed to understand how sieving affects FLD, and to relate FLD to sieve size in particular.

3. Image processing analysis

Two alternative methods were developed to characterise the FLD of a batch of flakes. This section describes the various steps of the methods, which will later be used to characterise the FLD of shredded scrap in Section 4.

The steps of the two methods, named *measured-orientation method* and *assumed-orientation method*, are detailed in Table 3 and Fig. 5. The differences between the two alternative methods are highlighted in Table 3 in italics.

Specifically, the measured-orientation method requires knowledge about the offcut layup (for step 4) and the identification of the fibre orientation of the top layer (for step 2b). The identification can either be performed automatically using fibre detection tools and image analysis or manually. The purpose of this study was not to develop these fibre detection tools, which is why the fibre orientation was determined manually. Although such a measurement method indirectly estimates the FLD in each flake, it is considered to be the correct FLD by definition based on the following assumptions:

Table 3
Description of the process steps of both methods. The cells in italic highlight the differences between the measured-orientation and assumed-orientation methods.

Measured-orientation method:	Assumed-orientation method:
Step 1: sample a batch of flakes from an initial population;	Step 1: sample a batch of flakes from an initial population;
Step 2a: capture photographs of the flakes — a diffuser box has been used for this purpose;	Step 2: capture photographs of the flakes;
Step 2b: identify the fibre orientation of the top layer — this was done manually here but can be possibly performed automatically;	—
Step 3: convert the pictures to binary images by thresholding the flakes;	Step 3: convert the pictures to binary images;
Step 4: generate arrays of lines oriented along the fibre direction(s) of each ply, which can be recovered from the scrap layup and the orientation of the top ply for known scrap;	*Step 4: generate arrays of lines for an arbitrary set of orientations: every* 10° *from* 10° *to* 180°*;*
Step 5: intersect the binary images and their respective arrays of lines;	Step 5: intersect the binary images and the arrays of lines;
Step 6: compute the line length distribution of the intersected images, which is the FLD.	Step 6: compute the line length distribution of the intersected images, which is the FLD.

1. the flakes are flat;
2. the crimp percentage, if any, is null;
3. the edges of the flakes are sharp;
4. the fibres are not bent or sheared in the flakes.

The corrections required for these assumptions are not taken into account and may be time-consuming to implement or unknown to the user of the method. In the case of the *C/PPS offcuts - 2nd type*, assumptions 1 and 4 are valid because the offcuts originate from (flat) press-consolidated laminates. The other types of offcuts were coming from the trimming of press-formed components, which means assuming 1 and 4 is less accurate. However, visual inspection of the flakes revealed a limited number of bent flakes. Assumption 3 was found to be mostly valid for the shredded flakes in this study (see Fig. 6). The variations induced by protruding fibres were very limited. Additionally, the crimp percentage of the 5-harness satin used in this study (see Section 2) is <0.5%, and thus negligible [35].

Contrary to the measured-orientation method, the assumed-orientation method disregards fibre orientation in the flakes by selecting an arbitrary set of fibre orientations (step 4). This way, the assumed-orientation method calculates an FLD that is independent of the actual flake layup. It does not require prior knowledge of the layup of the flakes, nor detection of the fibre orientation of the top layer. For this study, an angular increment of 10° was chosen, representing a virtually isotropic in-plane layup. The angle of 10° remained unchanged when different scrap or a different scrap layup was used. The angles are always measured in the reference orthonormal basis of the photographs (see (e_1, e_2) in Fig. 5). The effect of the angular increment on the resulting FLD was tested for all the following increments: $5°, 10°, 20°$ and $45°$. Increments $< 10°$ were found not to improve the accuracy of the method, and thus 10° was chosen for this study. Such a method evidently results in less accurate FLDs than when calculated with the measured-orientation method, but it can be adapted to any batch of flakes without prior knowledge about the scrap in question. Consequently, it is beneficial to determine its accuracy compared to the measured-orientation method. The first part of the following section will answer this problem.

4. Results and discussion

The various C/PPS offcuts were shredded and sieved, using the settings as detailed in Section 2: blade width, screen size and offcut size. Overall, most flakes had a shape resembling a parallelogram or a trapezoid as shown in Fig. 6, while the average flake size was found to vary with shredding settings.

The first subsection will address the reliability of the methods defined in Section 3, particularly the reliability of the assumed-orientation method in respect to its manual counterpart. Additionally, possible reasons that explain the discrepancy and similarity between these two methods will be discussed. Consecutively, the assumed-orientation method will be used to characterise FLDs in order to clarify which parameters affect FLDs and to which extent.

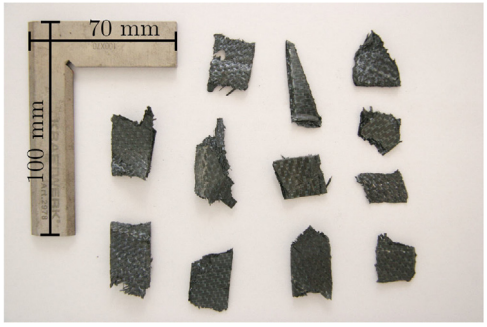

Fig. 6. Picture of some C/PPS flakes with a 70 mm × 100 mm set square.

4.1. Reliability study

Batches were sampled randomly for the two implemented methods. Since this may induce statistical variability, a reproducibility and repeatability study was performed first, using the measured-orientation method. Six kilogrammes of flakes were obtained from shredding *C/PPS 2nd type* using an RS30 with a 19 mm blade width and a 40 mm screen size. These were then kept stationary after shredding to prevent the finer particles from sinking to the bottom of the container. Seven batches were sampled without replacement, i.e. flakes were drawn once and not returned to the population, from the top of the container. The first five batches were sampled by the first operator and the last two by another operator on a different day.

4.1.1. Measured-orientation method

The FLDs of the seven batches were calculated using the measured-orientation method. Examples of such FLDs are shown in Fig. 7a, which can be characterised as a uni-modal distribution peaking at around 20 mm, which is close to the blade width of 19 mm. This apparent correlation will be discussed in further paragraphs. These distributions were found not to fit with regular probability density functions that might characterise FLDs, such as log-normal [17] or Weibull [36,37]. This is mostly due to the characteristic long tail and high peak of the presented FLDs. All seven batches resulted in FLDs similar to Fig. 7a. A correlation coefficient, r_N, based on the Pearson correlation coefficient, can be calculated to quantify this similarity [38]. Ideally, r_N would be the correlation coefficient between the FLD of batch number N and the FLD of the parent population. However, due to the difficulty of calculating the FLD of the entire population, the weighted average of the seven batches is considered to be the best approximation. Thus, r_N compares the FLD of each batch to this average:

$$r_N = \frac{\Sigma_{i=1}^{n}(x_{N,i} - \tilde{x}_N)(X_i - \tilde{X})}{\sqrt{\Sigma_{i=1}^{n}(x_{N,i} - \tilde{x}_N)^2 \Sigma_{i=1}^{n}(X_i - \tilde{X})^2}} \quad (1)$$

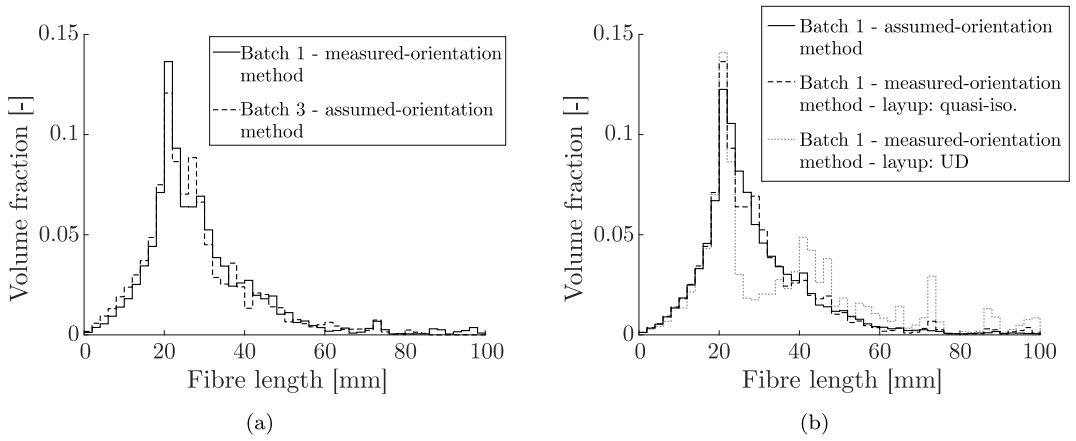

Fig. 7. Comparison of FLDs of batches calculated using the manual method or automatic method to show the correlations between batches and between methods.

Table 4
Correlation coefficients of the batches used for the reliability study as defined in Eqs. (1) and (2).

Batch	#1	#2	#3	#4	#5	#6	#7
r_N	0.985	0.990	0.985	0.980	0.991	0.978	0.986
Flakes per batch	63	63	64	61	93	59	60
$r_{quasi,N}$	0.986	0.990	0.975	0.989	0.961	0.973	0.982
$r_{cross,N}$	0.950	0.960	0.885	0.882	0.923	0.925	0.970
$r_{UD,N}$	0.854	0.907	0.696	0.811	0.853	0.904	0.896

where N refers to batch number N (from 1 to 7), $x_{N,i}$ is the length fraction (or volume in this case) of batch N for the fibre length i, $\tilde{x}_N$ refers to the arithmetic mean of all $x_{N,i}$ and X refers to the weighted average of the seven batches. Table 4 lists the r_N for the seven batches, which are all larger than 0.978. Even though these numbers are close to 1, it is difficult to objectively conclude whether they are large enough. As an example, Fig. 7a displays two FLDs that each have an r_N of 0.985, showing what level of variability is expected for such an r_N. To sum up, it can be concluded that the sampling method induces a low statistical variability from the r_N coefficients in Table 4 as well as from the FLDs displayed in Fig. 7a. It is also important to note that these levels of correlation can be achieved for small batches (Table 4), featuring between 59 and 93 flakes per batch. This improves the robustness of industrial recycling solutions. Batch-process routes, such as in [5,6,9], result in virtually identical FLDs from one batch to another.

4.1.2. Assumed-orientation method

Next, the assumed-orientation method was employed to calculate FLDs, which were compared to those computed with the measured-orientation method. As a reminder, the assumed-orientation method disregards the actual flake layup when computing FLDs. All the flakes in the current study are shredded quasi-isotropic offcuts. However, the industry uses or will use various layups to manufacture TPC components. Therefore, the accuracy of the assumed-orientation method must be tested against various flake layups. For that purpose, the actual layup of the seven batches of flakes was considered when analysing the flakes (the case presented in the previous paragraphs), or they were considered to have a virtual layup (cross-ply and unidirectional (UD)). The resulting FLDs for each layup configuration were then compared to the results of the assumed-orientation method. Correlation coefficients were calculated between the FLDs computed using the assumed-orientation method and the FLDs calculated with the measured-orientation method for each layup situation and for all seven batches. An expression of such a coefficient is defined as:

$$r = \frac{\Sigma_{i=1}^{n}(x_i - \tilde{x})(y_i - \tilde{y})}{\sqrt{\Sigma_{i=1}^{n}(x_i - \tilde{x})^2 \Sigma_{i=1}^{n}(y_i - \tilde{y})^2}} \quad (2)$$

where x and y refer to the two FLDs to be compared. Similarly to Eq. (1), x_i corresponds to the volume fraction for the fibre length i of the FLD represented by x, and $\tilde{x}$ is the arithmetic mean of all x_i. The various layups are denoted by $r_{quasi,N}$, $r_{cross,N}$ and $r_{UD,N}$. The names *quasi*, *cross* and *UD* refer to the layup (true or virtual) of the flakes when running the measured-orientation method. As before, N corresponds to the batch number, ranging from 1 to 7. Table 4 lists the results for these three coefficients for all batches and Fig. 7b shows a few typical FLDs to help visualise the correlation levels between the assumed-orientation method and the measured-orientation method for different layups.

Table 4 highlights that all $r_{quasi,N}$ and $r_{cross,N}$ coefficients are very high. The $r_{UD,N}$ coefficients, on the contrary, show some deviations, as they range from 0.70 to 0.91. The FLDs in Fig. 7b illustrate an example for batch 1, computed with a virtual UD layup on the one hand and with the assumed-orientation method on the other. This results in a mediocre correlation between the two FLDs, validated by $r_{UD,1} = 0.854$. Although the two FLDs look different, the major characteristics are well captured: a high peak at 20 mm, a very good correlation for fibres smaller than 20 mm and a long tail for long fibres.

Two main results can be derived from this study of the assumed-orientation method. Firstly, the assumed-orientation method can be used instead of the measured-orientation method, as it characterises FLDs well when flakes have a quasi-isotropic layup, which is the case in this study (see Section 2). Secondly, the results on $r_{quasi,N}$, $r_{cross,N}$ and $r_{UD,N}$ seem to show that flake layup hardly influences the FLD in most cases, as opposed to flake shape.

4.1.3. Discussion

The possible origins of the influence of flake layup and shape on the FLD are discussed here. First, flakes obtained from multiple-shaft shredders mainly look like parallelograms, or possibly quadrilaterals, as shown in Figs. 2b and 6. As offcuts might be shredded from any orientation, fibres might also have any orientation, irrespective of flake layup, indicated as θ in the referential of the flake (see Fig. 8). However, there are two phenomena limiting the influence of θ on FLD. To make matters simpler, consider a single rectangular flake. Fig. 8a illustrates that variations in fibre length ($\Delta L(\theta)$) are small when θ is small, whereas variations in $L(\theta)$ are large for large angles, in which θ is defined with respect to either of the principal directions of a parallelogram flake (e_1 and e_2 in Fig. 8). When the fibres are randomly oriented in the flakes, there will be many more fibres with a length close to the flake width and flake height. Consequently, the offcut layup has less influence on the FLD than the flake shape and size. Figs. 8b and 8c highlight the areas of constant fibre length in grey. It is clear from these figures that there are more fibres of length $L(\theta)$ for a small angle θ than for a large angle. This, again, indicates that there are more fibres

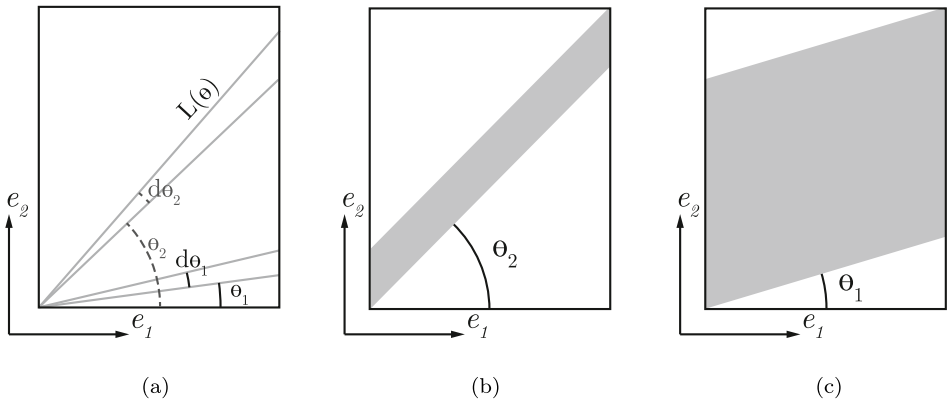

Fig. 8. Sub-Figs. 8a, 8b and 8c show two reasons that explain the minor influence of layup on FLDs and the presence of peaks in the FLDs (Fig. 7a): there are more fibres for small angles and the fibre length distribution is scattered when θ increases.

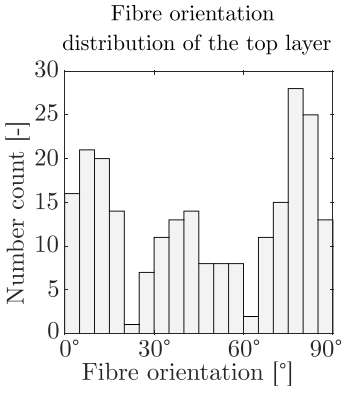

Fig. 9. Measured distribution of the fibre orientation of the top layer for the flakes of the batch number #5.

with a length close to the flake width and flake height when the fibres are randomly oriented in flakes.

These phenomena demonstrate that FLDs are dependent on flake size and shape as well as on the orientation in which the offcuts were shredded. However, the offcut layup has no influence when the orientation of the offcuts in the shredders is completely random. The shredding experiments performed in this study showed that this orientation seemed random if the hopper is large enough to be fed by offcuts in every orientation. Measurements were made for a batch of flakes that closely matches these conditions: *C/PPS offcuts — large* shredded with an RS40 shredder (test #5 in Table 2). The fibre orientation of the top layer was measured from pictures of the flakes. The orientation of flakes on the pictures was also set to be the 0° reference. A histogram plot of the results is shown in Fig. 9. The number of fibres is relatively low around 20°–25° and 60°–65°, while relatively high numbers of fibres are found at 0°, 45° and 90°. However, these peaks are fairly flat and most angles are well distributed. The offcuts used in this section, *C/PPS 2nd type*, have a much larger aspect ratio and were fed into the shredder less randomly. As a consequence, the orientation distribution of the top layer is more centred at 0° and 90°. Because of this, one would expect variations between the FLDs computed with the measured-orientation method for various flake layups. These differences are visible for the UD case (see Table 4). The $r_{UD,N}$ coefficients vary, indeed showing correlations that range between marginal and good. Still, the $r_{quasi,N}$ and $r_{cross,N}$ coefficients are high confirming that offcut layup has far less influence on FLD than flake size.

Additionally, the argument for a single rectangular flake can be extended to explain the shape of the FLDs. As there are more fibres with a length close to the flake width and flake height, it is expected that the FLD can be obtained from the distribution of flake width and height. This statement becomes more accurate for flakes with a high aspect ratio as it strengthens the two phenomena. It also remains true for variations in flake size, as there are independent of flake size. However, changes in flake shape can diminish the effects. This should be studied case by case and probably depends on flake convexity and the number of edges of the flake in question. One of the possible representations is to use maximum and minimum Feret diameters, which correspond to the maximum and minimum lengths of a random shape that can be measured with a calliper [39]. Fig. 10 shows the distribution of these minimum and maximum Feret diameters of flakes obtained from the image processing analysis. The distribution of the minimum Feret diameters is narrow, peaking at 22 mm, while the maximum Feret diameter ranges from 20 mm to 100 mm. This explains the peak at 20–22 mm in Fig. 7, obtained with a 19 mm blade width, as well as

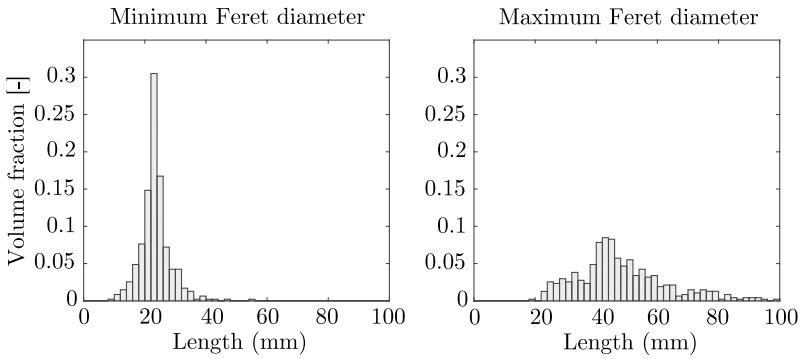

Fig. 10. Length distributions of the minimum and maximum Feret diameters for a batch of flakes, showing a narrow peak for the minimum diameter and a wide distribution for the maximum diameter.

the long tail next to this peak. The discrepancy between blade width and the minimum Feret diameter can be explained by various factors. On one hand, blade clearance and wear of the shredder may lead to slightly larger cuts than the expected 19 mm. On the other hand, the observed flakes have small protruding fibres or broken particles next to the flakes, which artificially increase the Feret diameters.

Nevertheless, the assumed-orientation method was shown to reliably capture FLDs of quasi-isotropic flakes.

4.2. The influence of shredding settings and sieving

The results of the previous section explained the development and reliability of the methods, especially the assumed-orientation method, which will be used for the rest of the study. These results enable us to proceed to the last aim of the paper: to understand whether and how, offcut size, shredding settings and sieving influence the FLD of the resulting flakes. Three cases are tested in this section.

- The first considers offcuts of different sizes shredded with the same parameters, to determine whether offcut size influences the FLD of the shredded flakes. Three offcut sizes were used for this purpose.
- The second case tests the influence of varying shredding parameters, namely blade width and screen size, on the FLD. Shredding experiments with four combinations of blade width and screen size were performed.
- The third case involves the sieving of shredded flakes, to determine the relation between sieve size and FLD. A set of different sieves was used to sieve one batch of flakes.

First, offcuts of the various sizes listed in Table 1 were shredded using an S20, a two-shaft shredder without a screen. The shredded output was fed through the shredder four times to create multiple cuts and to simulate the effect of a screen. A visual inspection revealed that slightly more fine particles were produced than with the four-shaft plus screen system. A single batch was sampled and analysed for each of the three offcut sizes. The corresponding FLDs are displayed in a boxplot in Fig. 11 (top three rows). The peak location is also indicated and is situated at 20 mm for all three cases, which was expected as the blade width is 19 mm (one of the dashed lines in Fig. 11). Besides, the scatter of the FLD, regardless of whether interquartile range or 90% spread is considered, is nearly constant. For comparison purposes, a correlation coefficient was calculated between the FLDs resulting from tests #1 & #3, and #2 & #3, following Eq. (2). This resulted in $r_{\#1,\#3} = 0.910$ and $r_{\#2,\#3} = 0.990$ respectively, which confirms their apparent correlation. Although FLDs shift slightly towards longer fibres when offcut weight increases, this effect is very limited compared to the differences between the average offcut weight and size (see Table 1).

Secondly, the shredding parameters of four-shaft shredders were varied while processing the same type of offcuts. The following combination of blade width [mm] and screen size [mm] were used: (29–25), (19–40), (29–40) and (29—no screen). The bottom four rows in Fig. 11 summarise the resulting FLDs, and one batch was sampled and analysed for each combination of settings. Similarly to the previous case, the peak value is equal to blade width when screen size, if applicable, is larger than the blade width (tests #5, #6 and #7). Otherwise, when the screen is smaller than the blade width, the shredded flakes had much smaller fibre lengths (tests # 4 and #6). This is a direct consequence of flakes being cut multiple times in the shredder before they pass through the screen. For those tests, flake area was also measured by means of image analysis, confirming the results. The average flake area for test #4 was 379 mm^2, while #5 and #6 resulted in 603 mm^2 and 950 mm^2 respectively. In addition, larger blade widths result in larger flakes and shift the bulk of FLDs to longer fibres (tests #5 and #6), as a result of increased flake size.

Overall, the seven FLDs in Fig. 11 show that the bulk of fibre lengths is narrowly distributed at the peak, in addition to having long tails on the right-hand side. This is in accordance with the findings of the previous section.

Thirdly, flakes shredded from C/PPS large offcuts (19 mm blade - no screen - 5 cuts) were sieved using a multi-stage vibrating sieve, as described in Section 2. One batch of flakes was sampled from the material resting on each sieve. The FLDs were calculated and are shown in Fig. 12 in a boxplot form. The aperture of the sieves from between which the flakes were retrieved, is overlaid on the FLDs. As expected, based on the results of the previous section, the FLDs are directly correlated to their related sieves. Flake size is linked to the sieve aperture, and so is the FLD. A small percentage of flakes did not pass through the 22.4 mm sieve. This may be due to the S20 shredding machine, to which no screen could be attached, which might produce these large flakes. The fraction of flakes retrieved from the 11.2 mm and 22.4 mm sieves represents 70%, which is in agreement with the expectations and previous results: most of the flakes have a size close to the blade width. The flakes resting on sieves of aperture 8 mm and lower start to delaminate when using this shredding system and these blade/screen parameters. Importantly, different comminution techniques may induce delamination of flakes at different flake sizes from what it observed here. This primarily depends on the dominant comminution mechanism, impact or shearing [15].

5. Conclusion

The objective of this paper was to develop and implement a new method that calculates FLD from a batch of multi-layered flakes. Recycling routes, such as those presented in [6] can benefit greatly from knowing the fibre lengths in the recyclate. The next step was to use this newly implemented image processing method to understand whether and how shredding parameters can influence FLD, as well as seeing how FLD could be adjusted by means of sieving.

In this study, an image processing method that disregards the actual flake layup was successfully implemented and used to calculate FLDs from pictures of flakes. It was found that FLD is closely related to flake size and is barely affected by offcut layup, if the offcuts are fed into the shredder at random orientations. This characteristic extends the validity of the method to shredded composites when there is no prior knowledge of the layup. However, the methods and the results remain valid only if flakes do not delaminate during the shredding process.

Additionally, the researchers noticed that production scrap can vary in size. However, this was shown to have no influence on FLD/PSD, which is a significant result when setting up a pilot plant or production line to recycle collected scrap. Along the same lines, it was demonstrated that sampling batches from a population of shredded flakes is reproducible even when batches are as small as 60 flakes. Such a stable FLD/PSD, from batch to batch or in a continuous process, will be a minimum prerequisite for any application requiring reproducible part performance.

Finally, it was shown that changing the blade width and screen shifted FLD location and peak, as well as modifying the overall scatter of FLDs. Sieving provides a simple way to separate fine and coarse particles. It was also found that the aperture size of the sieves is closely correlated to the FLD of flakes resting on each sieve. These results were obtained with flakes shredded from quasi-isotropic offcuts but the authors believe that similar results can be expected if the scrap layup varies.

This study focused on TPCs, but the results presented here, as well as the assumed-orientation method, can be easily used for the recycling of thermoset composites. Although recycling solutions for thermoset composites are different from those for TPCs, the comminution step can be similar, which results in similar needs to characterise FLDs.

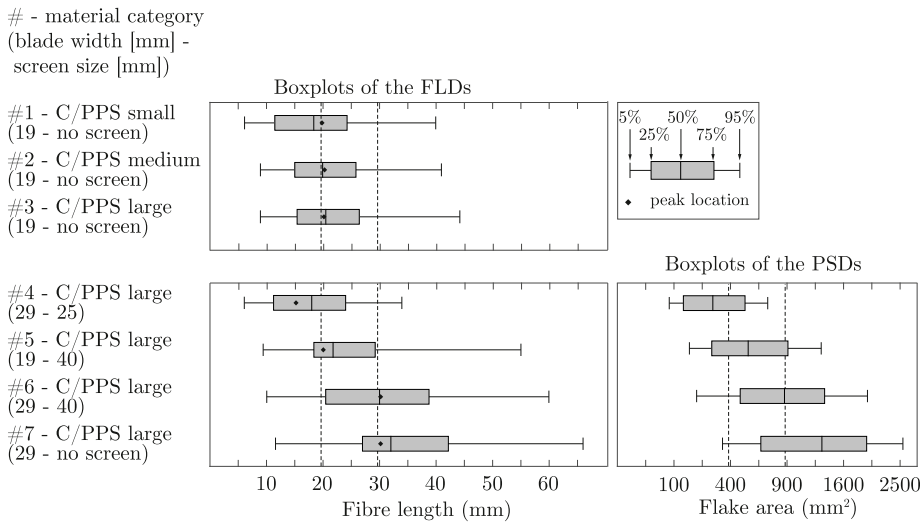

Fig. 11. FLDs (left) and PSDs (right) of various flakes in a boxplot form. The first three rows illustrate variations of FLD when the offcuts vary in size, whereas the last four rows correspond to flakes shredded with various settings. The dashed lines at 19 mm and 29 mm highlight the blade width of the shredders used in this study.

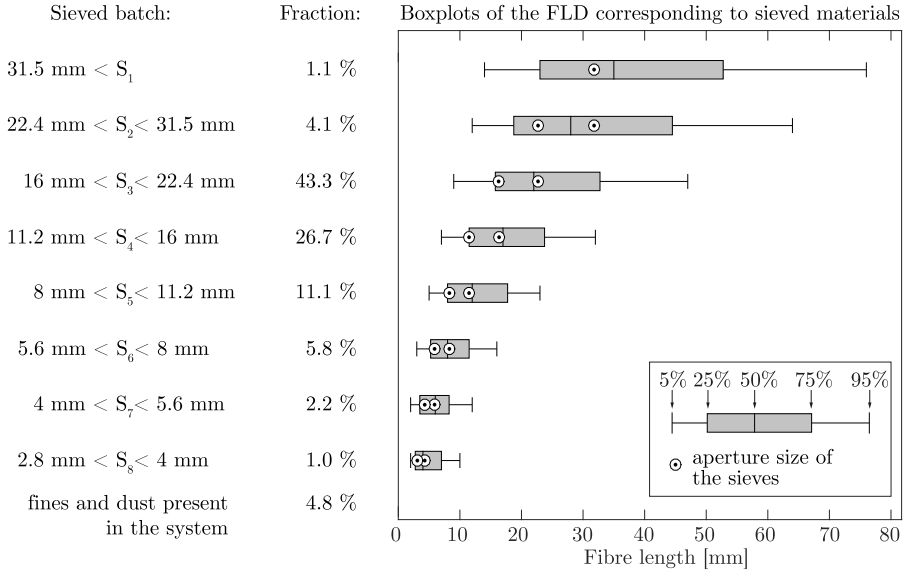

Fig. 12. Boxplots of the FLDs of sieved flakes. Each row corresponds to flakes resting on each sieve of the multi-stage sieve. The apertures of the corresponding sieves, which are written on the left-hand side, are indicated with round symbols over the boxplots.

Acknowledgements

This project was financed by the Dutch Organisation of Applied Research – SIA, through the project grant SIA-RAAK 2014-01-72PRO. The authors are grateful to the project partners: Toray Advanced Composites, GKN Aerospace's Fokker Business, Cato Composite Innovations, Dutch Thermoplastic Components and Nido RecyclingTechniek; as well as UNTHA shredding technology GmbH for shredding some of our materials.

References

[1] CompositesWorld. Thermoplastic composites: Past the tipping point?, 2018. https://www.compositesworld.com/articles/thermoplastic-composites-past-the-tipping-point, [Online; accessed 18-January-2019].

[2] The Council of European Union. Directive 1999/31/EC on the landfill of waste, 1999.

[3] The Council of European Union. Directive 2000/53/EC on end-of life vehicles, 2000.

[4] Abdul Rasheed MI. Compression molding of chopped woven thermoplastic composite flakes: A study on processing and performance. (Ph.D. thesis), University of Twente; 2016.

[5] De Bruijn TA, Vincent GA, Van Hattum FWJ. Recycling of long fibre thermoplastic composites by low shear mixing. In: SAMPE Europe. 2016.

[6] De Bruijn TA, Vincent GA, Van Hattum FWJ. Recycling C/PPS laminates into long fibre thermoplastic composites by low shear mixing. In: 21st International Conference in Composite Materials. 2017.

[7] Roux M, Eguemann N, Dransfeld C, Thiebaud F, Perreux D. Thermoplastic carbon fibre-reinforced polymer recycling with electrodynamical fragmentation: From cradle to cradle. J. Thermoplastic Composite Mater. 2015.

[8] Toho Tenax. Green Innovations, https://www.teijincarbon.com/products/green-innovations/, [Online; accessed 19-April-2018].

[9] Moothoo J, Ouagne P. Mechanical recycling of continuous fibre reinforced thermoplastic composites using compression moulding. In: 17th European Conference on Composite Materials. 2016.

[10] Schinner G, Brandt J, Richer H. Recycling carbon-fiber-reinforced thermoplastic composites. J. Thermoplastic Composite Mater. 1996;9(3):239–45.

[11] Cetim. Thermosaïc®, http://www.cetim-cermat.com/fr/technologie-thermosaic/, [Online; accessed 23-August-2018].

[12] TenCate Advanced Composites Cetex®Recycling Thermoplastic Composites, https://www.tencatecomposites.com/media/e0c5c4b6-10bc-4aee-9649-5f94bd793504/XNg0sw/TenCate [Online; accessed 23-August-2018].

[13] Vaidya U, Thattaiparthasarthy KB, Pillay S, Ning H. Automotive applications with cost-effective and recycled thermoplastic composites. In: International SAMPE Technical Conference. 2012.
[14] Li H, Englund K. Recycling of carbon fiber-reinforced thermoplastic composite wastes from the aerospace industry. J. Compsite Mater. 2017;51.
[15] Biddulph MW. Principles of recycling processes. Conserv. Recycl. 1976;1(1):31–54.
[16] Thomason JL. The influence of fibre length and concentration on the properties of glass fibre reinforced polypropylene: 5. injection moulded long and short fibre PP. Composites A 2002;33(12):1641–52.
[17] Van Hattum FWJ, Bernardo CA. A model to predict the strength of short fiber composites. Polym Compos 1999;20(4):524–33.
[18] Goris G, Back T, Yanev A, Brands D, Drummer D, Osswald TA. A novel fiber length measurement technique for discontinuous fiber-reinforced composites: A comparative study with existing methods. Polym Compos 2017;39(11).
[19] Fu S-Y, Mai Y-W, Ching EC-Y, Li RKY. Correction of the measurement of fiber length of short fiber reinforced thermoplastics. Composites A 2002;33(11):1549–55.
[20] Bernasconi A, Rossin D, Armanni C. Analysis of the effect of mechanical recycling upon tensile strength of a short glass fibre reinforced polyamide 6,6. Eng Fract Mech 2007;74(4):627–41.
[21] Mativenga PT, Shuaib NA, Howarth J, Pestalozzi F, Woidasky J. High voltage fragmentation and mechanical recycling of glass fibre thermoset composite. CIRP Ann. - Manuf. Technol. 2016;65(1):45–8. http://dx.doi.org/10.1016/j.cirp.2016.04.107.
[22] Pickering SJ, Kelly RM, Kennerley JR, Rudd CD, Fenwick NJ. A fluidised-bed process for the recovery of glass fibres from scrap thermoset composites. Compos Sci Technol 2000;60(4):509–23.
[23] Turner TA, Pickering SJ, Warrior NA. Development of recycled carbon fibre moulding compounds - preparation of waste composites. Composites B 2011;42(3):517–25.
[24] Palmer J. Mechanical recycling of automotive composites for use as reinforcement in thermoset composites. (Ph.D. thesis), University of Exeter; 2009.
[25] Rouholamin D, Shyng YT, Savage L, Ghita OR. A comparative study into mechanical performance of glass fibres recovered through mechanical grinding and high voltage pulse power fragmentation. In: 16th European Conference on Composite Materials. 2014.
[26] Beauson J, Madsen B, Toncelli C, Brø nsted P, Bech JI. Recycling of shredded composites from wind turbine blades in new thermoset polymer composites. Composites A 2016;(90).
[27] Shuaib NA, Mativenga PT. Effect of process parameters on mechanical recycling of glass fibre thermoset composites. Proc. CRIP 2016;(48).
[28] Benoit N. Mechanical recycling of high density polyethylene/flax fiber composites. (Ph.D. thesis), Canada: University of Laval; 2017.
[29] Abdul Rasheed MI, Rietman B, Visser HA, Akkerman R. Experimental characterisation of recycled (glass/TPU woven fabric) flake reinforced thermoplastic composites. In: 19th International Conference in Composite Materials. Montreal, Canada; 2013, p. 3999–4010.
[30] Pickering SJ. Thermal methods for recycling waste composites. In: Goodship V, editor. Management, Recycling and Reuse of Waste Composites. Woodhead Publishing; 2010, chapter 4.
[31] Woldt D. Zerkleinerung nicht-spröder Stoffe in Rotorscheren. (Ph.D. thesis), TU Bergakademie Freiberg; 2003, p. 122.
[32] UNTHA shredding technology Gmbh. Rs30/40 datasheet http://www.untha.com/files/pdf/brochures/en/machines/holz_en_rs30-40-wood-shredder.pdf, [Online; accessed 23-August-2018].
[33] UNTHA shredding technology Gmbh. Rs50/60/100 datasheet http://www.untha.com/files/pdf/brochures/en/machines/rs50-100_industrial-shredder_en_8seitig.pdf, [Online; accessed 23-August-2018].
[34] European Commission. Recommendation from the Scientific Committee on Occupational Exposure Limits for man made-mineral fibres (MMMF) with no indication for carcinogenicity and not specified elsewhere, 2012.
[35] Horrods AR, Anand SC. Handbook of Technical Textiles. CRC Press; 2000.
[36] Masubuchi Y, Terada M, Yamanaka A, Yamamoto T, Ishikawa T. Distribution function of fiber length in thermoplastic composites. Compos Sci Technol 2016;134:43–8.
[37] Turner TA, Warrior NA, Pickering SJ. Re-use of carbon fibres in high value moulding compounds & pre-pregs. Polym Compos 2009.
[38] Press WH, Teukolsky SA, Vetterling WT, Flannery BP. Statistical description of data. In: Numerical Recipes in C: The Art of Scientific Computing. 1992, p. 949.
[39] Jillavenkatesa A, Dapkunas SJ, Lum L-SH. Particle size characterization. NIST. 2001.